Charge retention characteristics of silicon nanocrystal layers by ultrahigh vacuum atomic force microscopy

Tao Feng,[a] Gerald Miller, and Harry A. Atwater
Thomas J. Watson Laboratory of Applied Physics, California Institute of Technology, Pasadena, California 91125

(Received 1 March 2007; accepted 13 June 2007; published online 8 August 2007)

The nanoscale charge retention characteristics of both electrons and holes in SiO_2 layers containing silicon nanocrystals were investigated with ultrahigh vacuum conductive-tip noncontact atomic force microscopy. The results revealed much longer hole retention time (e.g., >1 day) than that of electrons (e.g., ~1 h). A three-dimensional electrostatic model was developed for charge quantification and analysis of charge dissipation. Based on the superior retention characteristics of holes, a *p*-channel nanocrystal memory working with holes is suggested to be an interesting choice in improving data retention or in further device scaling. © *2007 American Institute of Physics*. [DOI: 10.1063/1.2764001]

I. INTRODUCTION

With discrete nanocrystals as charge storage nodes, silicon nanocrystal memory[1,2] shows a strong immunity to charge leakage problem, making further device scaling possible. The reduced oxide thickness may bring lower operation voltages, lower power consumption, and better endurance characteristics. In addition, silicon nanocrystal memory can be fabricated with current complementary metal-oxide semiconductor (CMOS) technology.[3] On the road to commercialization, however, superior charge retention still needs to be demonstrated, and scaling limit needs to be well understood. As good tools for microscopic charge analysis, conductive-tip noncontact atomic force microscopy (nc-AFM)[4] and electrostatic force microscopy (EFM)[5] are very sensitive to electrostatic interaction due to even a small number of basic charges down to a single electron.[4] By using lift mode scanning with detection of frequency shift, Ng *et al.*[6] investigated the influence of Si nanocrystal distribution on charge decay rates, and Krishnan *et al.*[7] observed the effect of oxidation on charge localization and transport in a Si nanocrystal layer. We show from charge injection and imaging experiments by conductive-tip nc-AFM in an ultrahigh vacuum (UHV) chamber that holes have much longer retention time than electrons in Si nanocrystal layer fabricated through ion implantation.

II. SAMPLES AND EXPERIMENT

The samples were fabricated by implanting 5 keV Si^+ ions into 100 nm SiO_2 films grown on *p*-Si (100) substrates to a fluence of 1.27×10^{16} cm^{-2} ("high dose"), followed by thermal annealing at 1080 °C in Ar for 15 min to precipitate nanocrystals. The peak of Si distribution was simulated to be at 10 nm below the sample surfaces. In addition, a slightly lower ion-implantation dose (0.95×10^{16} cm^{-2}, or "low dose") was also selected to evaluate nanocrystal density dependence of charge retention. For comparison, control samples without implantation, or with implantation but without thermal annealing, were prepared.

Si nanocrystals formed under these implantation and annealing conditions cannot be easily resolved in transmission electron microscopy. In our previous work,[8] the structure characterization was provided by UHV scanning tunneling microscopy (STM) measurements on samples in which a thin oxide layer was fully etched with buffered hydrofluoric acid. Areal density of nanocrystals was found to be at least about 4×10^{12} cm^{-2}. Considering the loss of nanocrystals during the etching process, this value is a lower bound. By using UHV nc-AFM on etched samples further treated in an ultrasonic bath to lower the nanocrystal density [Fig. 1(a)], the

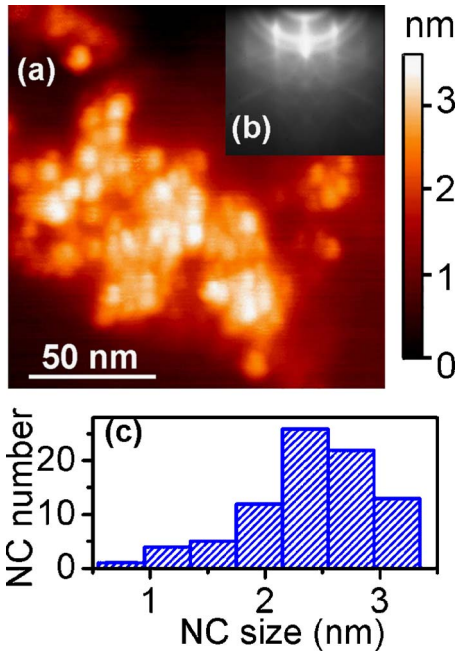

FIG. 1. (Color online) Structural characterization of ion-beam-synthesized Si nanocrystals on Si substrate. Si nanocrystals and Si substrate were exposed by SiO_2 etching. (a) nc-AFM images. (b) RHEED pattern. (c) Size distribution of Si nanocrystals.

[a]Electronic mail: tfengca@gmail.com

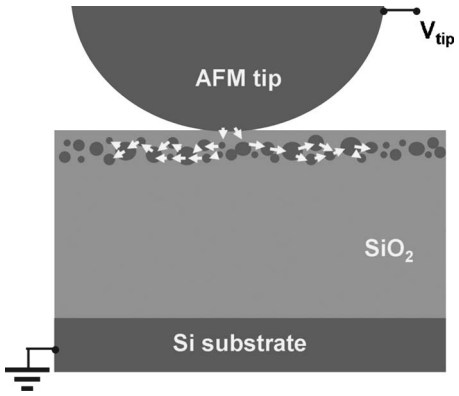

FIG. 2. Schematic of charge injection into a silicon nanocrystal layer with a biased conductive AFM tip.

vertical sizes of most nanocrystals were observed to be 1.5–3.5 nm [Fig. 1(c)]. The average size is about 2.5 nm. An upper bound on nanocrystal areal density can be derived from the average nanocrystal size and the total fluence of implanted Si^+ ions, and is estimated to be in the range of 10^{13} cm^{-2}. In the above analysis, nanocrystals were assumed to be spherical so that nanocrystal vertical size obtained from nc-AFM was used as diameter. However, it should be noted that this assumption only works for a rough estimation and may not be accurate, especially when the implantation fluence is larger than a "percolation threshold."[9] Detection of nonspherical nanocrystals has been reported with high-resolution cross-sectional transmission electron microscopy (XTEM) method.[10] Figure 1(b) shows the pattern of reflection high-energy electron diffraction (RHEED) for an etched nanocrystal sample. In addition to diffraction spots and Kikuchi lines due to single-crystalline substrate, diffraction rings can be clearly observed, which confirms the crystallinity of the nanoparticles detected in STM and nc-AFM.

Charge injection and imaging experiments were performed with a UHV nc-AFM.[11] The pressure inside the UHV chamber was around 10^{-9} Torr, which not only excluded the influence of surface water and other contamination as charge storage media and dissipation paths, but also increased charge detection sensitivity and stability due to lack of air damping. An n^+-doped Si cantilever with a force constant of 42 N/m and a resonant frequency of 284 kHz was used. During charge injection, a tip bias of +10 V or −10 V with respect to grounded sample substrate was applied for 10 s (Fig. 2). The charge injection process is similar to the charging process of a parallel capacitor, except that charging in the top plate, or the nanocrystal layer, is nontrivial only within a certain distance, resulting in a disk-shaped charged area. After charge injection, the tip was retracted and continuous scans in noncontact mode ($\Delta f = -30$ Hz) were performed to monitor the charge dissipation process in real time. It should be noted that the oxide layer underneath nanocrystals was selected to be much thicker than that used in a real device to enable a sufficiently large charging area in the charge injection and to avoid a strong substrate screening effect in charge detection.

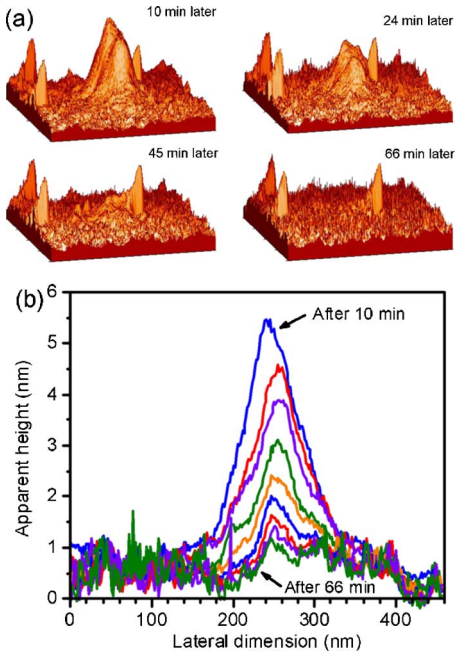

FIG. 3. (Color online) (a) nc-AFM images acquired after charge injection into the "low dose" nanocrystal sample with a tip bias of −10 V for 10 s. The scanned area is 400×400 nm^2. (b) Series of line profiles through the center of the protrusion, which were recorded with an interval of 7 min.

III. RESULTS AND ANALYSIS

A tip bias of −10 V was applied for 10 s to inject electrons into SiO_2 films containing Si nanocrystals. The electron injection and imaging experiments were tried with the high dose nanocrystal sample, but no charge could be detected even in the first scan performed 10 min after the injection. However, when the experiments were repeated with the low dose nanocrystal sample, localized charge was detected. Figure 3 shows a series of nc-AFM images. In the first image that was taken 10 min after charge injection, there is a protrusion with a height of 5.5 nm. In the following scans the protrusion height decreased continuously. So it is fairly clear that the protrusion was due to electrostatic interaction between the doped Si tip and injected electrons. After around 1 h, the protrusion almost disappeared, indicating that the remaining charge was close to the AFM detection limit. In contrast, there were three smaller protrusions with no change in shape and height. We believe that these invariant features were due to small debris dropped off from the tip during the charging period. Because of the tip convolution effect, tip shape, rather than shape of the small debris, was recorded.

A tip bias of +10 V was applied for 10 s to inject holes. In subsequent charge imaging, localized holes were detected in both high and low dose nanocrystal samples. Figure 4 shows nc-AFM images obtained after injection of holes into the high dose sample. In the first image taken about 12 min after the injection of holes, a large protrusion with a height of more than 30 nm and full-width half maximum (FWHM) of around 150 nm was observed, indicating much more total injected charge than that in the electron charging experiment. Since then, it took 2.2, 4.9, and 18.4 h for the peak height to drop to approximately 50%, 25%, and 12.5% of the initial value, respectively. Holes show better retention characteris-

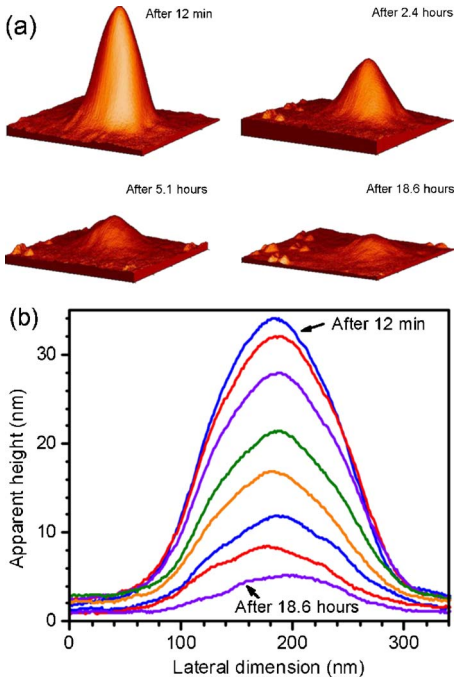

FIG. 4. (Color online) (a) nc-AFM images acquired after charge injection into the "high dose" nanocrystal sample with a tip bias of +10 V for 10 s. The scanned area is 400×400 nm^2. (b) Series of line profiles through the center of the protrusion, which correspond to charge dissipation time of 0.2, 0.4, 0.75, 1.6, 2.4, 3.5, 5.1, and 18.6 h, respectively.

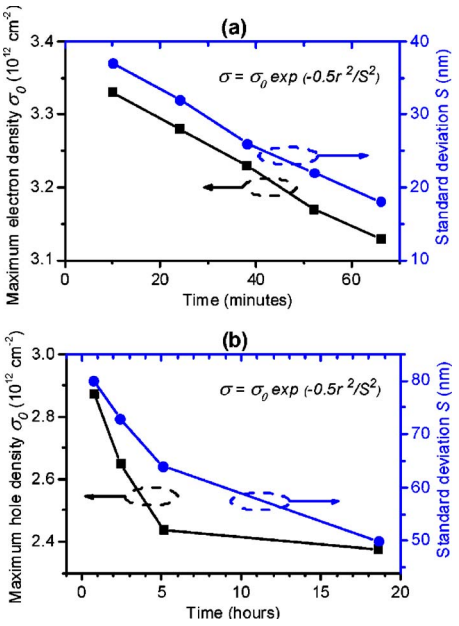

FIG. 5. (Color online) Evolution of Gaussian charge distributions in Si nanocrystal layer acquired from 3D electrostatic simulation. (a) and (b) correspond to discharging series in Figs. 3 and 4, respectively.

tics than electrons. In the hole charging experiments with the low dose sample, no obvious decay can be observed, making it infeasible to monitor major charge dissipation process at room temperature.

To identify the location of the trapped charge, control samples were also investigated. No electron was detected on any control sample; holes were detected on all control samples, but with smaller apparent height and shorter retention time than the data for nanocrystal samples. In the hole charging experiment on a SiO_2 control sample, it took 1.5 h for protrusion height to decay from 9.5 nm to less than 1 nm. The fast dissipation process of surface charge shows that the majority of the injected charge in the nanocrystal samples was not trapped in surface states. After the charging of holes into a high dose control sample, it took 4.1 h for the protrusion height to decay from 23 nm to less than 3 nm. Compared with the SiO_2 control sample, more holes were detected and the dissipation was slower, revealing that most holes were not located at sample surface, either. According to Boer *et al.*, charge may be trapped in or on Si nanocrystals, or in surface states, but not in bulk oxide defects.[12] So holes in the ion-implanted control sample were likely trapped in Si-related defects, amorphous Si clusters, or even very small Si nanocrystals that precipitated directly in ion implantation.[13] Compared with nanocrystals formed in high-temperature annealing, the average size of these nanoclusters is smaller, which also means smaller average spacing and stronger Coulomb blockade effect, so the charge retention time of the ion-implantation control sample is shorter than the corresponding nanocrystal sample. Since both surface states and Si-related defects constitute faster charge dissipation paths than the nanocrystal layer, it is reasonable that no electron charging could be detected in control samples.

UHV nc-AFM guarantees high detection sensitivity and stability in charge imaging experiments due to lack of air damping; so, a three-dimensional (3D) electrostatic model can be developed to provide a good estimation of charge distribution and evolution. The interactions between the Si tip and a charged sample include van de Waals force and electrostatic force.[12] Force gradient changes the cantilever's apparent spring constant and resonant frequency, and the change of resonant frequency shift is a preset parameter in nc-AFM operation. By using the model for noncontact mode,[14] the dynamic problem can be simulated by obtaining a curved surface with a constant force gradient,

$$\left(\frac{\partial F_z}{\partial z}\right)_{\text{total}} = \left(\frac{\partial F_z}{\partial z}\right)_{\text{vdW}} + \left(\frac{\partial F_z}{\partial z}\right)_{\text{electrostatic}} \approx -2k\frac{\Delta\omega_0}{\omega_0}. \tag{1}$$

To extract information regarding charge distribution from nc-AFM signals, an iterative method was used. In each time, a two-dimensional charge distribution at 10 nm underneath the sample surface was assumed, and the corresponding nc-AFM image was calculated and compared with experimental data, followed by a revision of the charge distribution based on the comparison. Such steps were repeated until a satisfactory match was achieved.

In simulation, Gaussian charge distributions generated a satisfactory match in most cases. Figure 5 shows the evolution of charge distributions in Si nanocrystal layers, which corresponds to the discharging series in Figs. 3 and 4, respectively. It was noticed that charge dissipation was primarily associated with decrease, rather than increase, of standard deviations of the Gaussian charge distributions. Considering that lateral charge dissipation in the nanocrystal layers is likely dominant due to the thick oxide, the evolution of

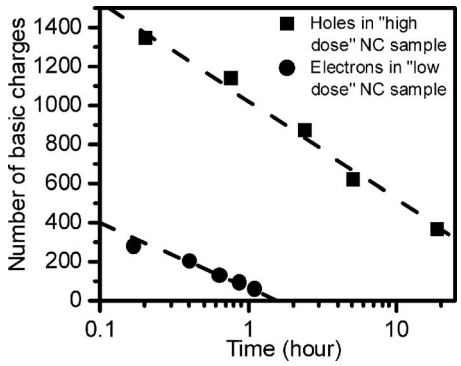

FIG. 6. Number of holes and electrons in the nanocrystal layers as a function of time acquired from 3D electrostatic simulation. The dashed lines are a guide for the eyes.

Gaussian distribution indicates that charge dissipates much faster where charge density is lower. This feature can be explained by the Coulomb blockade effect on tunneling paths. The fastest dissipation happens on the periphery of charge distribution with the lowest charge density, while redistribution within the area is much slower, resulting in continuous shrinkage of the charge distribution detectable by AFM tip. For the same reason, there was only a minor decrease in maximum charge density, which was around 3×10^{12} cm^{-2}, less than the areal density of nanocrystals. This result indicates less than a single charge per nanocrystal on average, which is again consistent with large Coulomb charging energy for such small nanocrystals. A more detailed analysis on charge dissipation mechanisms in Si nanocrystal layers based on the dissipation process of holes will be reported in another publication.

Figure 6 shows the calculated number of electrons and holes in nanocrystal layers as a function of time. The logarithmic time dependence of total charge was observed. By extrapolating the data in Fig. 6, hole retention time is nearly two orders of magnitude longer than electron retention time. The actual difference is even larger, since the difference in nanocrystal density needs be taken into account. The charge retention characteristics directly observed in nanoscale are consistent with previous data obtained by capacitance-voltage measurements on nanocrystal floating gate MOS capacitors.[8,15,16] In theory, holes having much better retention characteristics than electrons can be explained by the difference in tunneling barrier heights, 3.1 and 4.7 eV for electrons and holes, respectively. The retention times are also influenced by carrier effective mass in tunneling.

In the conventional continuous floating gate memory with relatively thick tunnel oxide, electrons are commonly selected as stored charge. By replacing the continuous floating gate with discrete Si nanocrystals, very thin tunnel oxide can be applied, thus making programming with holes possible.[17] In addition to good retention characteristics, the small lateral dissipation rate helps to keep holes underneath the gate area. All these advantages show that nanocrystal memory programming with holes is an interesting choice. A major concern regarding this concept is hole-induced oxide degradation. However, it was found that cold hole injection from inversion layer does not affect oxide reliability.[18] Endurance characteristics of a *p*-channel Si nanocrystal memory device working with low-energy holes in a direct tunneling regime did not show hot carrier degradation within 10^5 write/erase cycles.[17] More work is needed to further test the feasibility of the *p*-channel Si nanocrystal memory.

IV. CONCLUSION

UHV conductive-tip nc-AFM was used to inject charge into ion-beam synthesized Si nanocrystal layer and directly monitor subsequent charge dissipation. This effective tool for nanoscale charge analysis may help to determine whether Si nanocrystal memory can be a feasible choice for further device scaling into a few tens of nanometers regime. The charge retention characteristics showed logarithmic time dependence and were observed to depend strongly on nanocrystal areal density, as well as the type of injected charge. The superior retention characteristics of holes make nanocrystal memory programming with holes an interesting choice in improving data retention or in further device scaling.

[1] S. Tiwari, F. Rana, H. Hanafi, A. Hartstein, E. F. Crabbé, and K. Chan, Appl. Phys. Lett. **68**, 1377 (1996).
[2] R. Muralidhar *et al.*, Tech. Dig. - Int. Electron Devices Meet., p. 601 (2003).
[3] J. De Blauwe, IEEE Trans. Nanotechnol. **1**, 72 (2002).
[4] R. Stomp, Y. Miyahara, S. Schaer, Q. Sun, H. Guo, and P. Grutter, Phys. Rev. Lett. **94**, 056802 (2005).
[5] T. Mélin, H. Diesinger, D. Deresmes, and D. Stiévenard, Phys. Rev. Lett. **92**, 166101 (2004).
[6] C. Y. Ng, T. P. Chen, M. S. Tse, V. S. W. Lim, S. Fung, and A. A. Tseng, Appl. Phys. Lett. **86**, 152110 (2005).
[7] R. Krishnan, Q. Xie, J. Kulik, X. D. Wang, S. Lu, M. Molinari, Y. Gao, T. D. Krauss, and P. M. Fauchet, J. Appl. Phys. **96**, 654 (2004).
[8] T. Feng, H. B. Yu, M. Dicken, J. R. Heath, and H. A. Atwater, Appl. Phys. Lett. **86**, 033103 (2005).
[9] T. Müller, K. H. Heinig, and W. Möller, Appl. Phys. Lett. **81**, 3049 (2002).
[10] C. Bonafos *et al.*, J. Appl. Phys. **95**, 5696 (2004).
[11] Variable Temperature Ultrahigh Vacuum STM/AFM, Omicron Nanotechnology GmbH.
[12] E. Boer, M. L. Brongersma, H. A. Atwater, R. C. Flagan, and L. D. Bell, Appl. Phys. Lett. **79**, 791 (2001).
[13] C. J. Nicklaw *et al.*, IEEE Trans. Nucl. Sci. **47**, 2269 (2000).
[14] E. A. Boer, L. D. Bell, M. L. Brongersma, and H. A. Atwater, J. Appl. Phys. **90**, 2764 (2001).
[15] S. Huang, S. Banerjee, R. T. Tung, and S. Oda, J. Appl. Phys. **93**, 576 (2003).
[16] C. Busseret, A. Souifi, T. Baron, G. Guillot, F. Martin, M. N. Semeria, and J. Gautier, Superlattices Microstruct. **28**, 493 (2000).
[17] K. Han, I. Kim, and H. Shin, IEEE Trans. Electron Devices **48**, 874 (2001).
[18] K. Deguchi, S. Uno, A. Ishida, T. Hirose, Y. Kamakura, and K. Taniguchi, Tech. Dig. - Int. Electron Devices Meet., p. 327 (2000).